Neuron
Neurotechnique

Transcranial Pulsed Ultrasound Stimulates Intact Brain Circuits

Yusuf Tufail,[1] Alexei Matyushov,[1] Nathan Baldwin,[2] Monica L. Tauchmann,[1] Joseph Georges,[1] Anna Yoshihiro,[1]
Stephen I. Helms Tillery,[2,3,4] and William J. Tyler[1,2,*]
[1]School of Life Sciences
[2]Harrington Program in Bioengineering
[3]School of Biological and Health Systems Engineering
[4]Department of Kinesiology
Arizona State University, Tempe, AZ 85287, USA
*Correspondence: wtyler@asu.edu
DOI 10.1016/j.neuron.2010.05.008

SUMMARY

Electromagnetic-based methods of stimulating brain activity require invasive procedures or have other limitations. Deep-brain stimulation requires surgically implanted electrodes. Transcranial magnetic stimulation does not require surgery, but suffers from low spatial resolution. Optogenetic-based approaches have unrivaled spatial precision, but require genetic manipulation. In search of a potential solution to these limitations, we began investigating the influence of transcranial pulsed ultrasound on neuronal activity in the intact mouse brain. In motor cortex, ultrasound-stimulated neuronal activity was sufficient to evoke motor behaviors. Deeper in subcortical circuits, we used targeted transcranial ultrasound to stimulate neuronal activity and synchronous oscillations in the intact hippocampus. We found that ultrasound triggers TTX-sensitive neuronal activity in the absence of a rise in brain temperature (<0.01°C). Here, we also report that transcranial pulsed ultrasound for intact brain circuit stimulation has a lateral spatial resolution of approximately 2 mm and does not require exogenous factors or surgical invasion.

INTRODUCTION

All currently implemented approaches to the stimulation of brain circuits suffer from a limitation or weakness. Pharmacological and chemical methods lack brain target specificity and have numerous metabolic requirements. Electrical methods, such as deep-brain stimulation, offer a higher targeting specificity but require surgery and brain impalement with electrodes (Ressler and Mayberg, 2007). Optogenetic-based methods using light-activated ion channels or transporters offer unrivaled spatial resolution but require genetic alteration (Szobota et al., 2007; Zhang et al., 2007). Transcranial magnetic stimulation (TMS) and transcranial direct current stimulation do not require invasive procedures but suffer from poor spatial resolution of ≈1 cm (Barker, 1999; Wagner et al., 2007). Considering the above limitations, a remaining challenge for neuroscience is to develop improved stimulation methods for use in intact brains. To address this need, we began studying the influence of pulsed ultrasound (US) on neuronal activity in mice.

Ultrasound is a mechanical pressure wave (sound wave) having a frequency above the range of human hearing (>20 kHz). Due to its physical properties, specifically its ability to be transmitted long distances through solid structures, including bone and soft tissues, US is used in a wide range of medical and industrial applications. Diagnostic imaging US has a frequency range from 1 to 15 MHz, while therapeutic US tends to employ a frequency of about 1 MHz (O'Brien, 2007). Ultrasound can be transmitted into tissues in either pulsed or continuous waveforms and can influence physiological activity through thermal and/or nonthermal (mechanical) mechanisms (Dalecki, 2004; Dinno et al., 1989; O'Brien, 2007; ter Haar, 2007). The potential of using US for brain stimulation has been largely overlooked in comparison to chemical, electrical, magnetic, or photonic methods. Surprisingly, this is in lieu of the fact that US was shown capable of exciting nerve and muscle more than eight decades ago (Harvey, 1929).

Edmund Newton Harvey first published a set of groundbreaking observations that clearly described that US can stimulate nerve and muscle fibers in neuromuscular preparations (Harvey, 1929). Since then, US has been shown to stimulate and inhibit neuronal activity under various conditions. For example, US has been reported to reversibly suppress sensory-evoked potentials in the cat primary visual cortex following treatment of the lateral geniculate nucleus with US transmitted through a cranial window (Fry et al., 1958). Conversely, US has been shown to stimulate auditory nerve responses in the craniotomized cat brain (Foster and Wiederhold, 1978). In cat saphenous nerve preparations, US was shown to differentially modulate the activity of Aδ- and C-fibers, depending on the fiber diameter, US intensity, and US exposure time (Young and Henneman, 1961).

Ultrasound can be defined as low or high intensity (ter Haar, 2007). High-intensity US (>1 W/cm^2) influences neuronal excitability by producing thermal effects (Tsui et al., 2005). In addition to the initial studies cited above, high-intensity US has been reported to modulate neuronal activity in peripheral nerves (Lele, 1963; Mihran et al., 1990; Tsui et al., 2005), craniotomized cat and craniotomized rabbit cortex (Velling and Shklyaruk, 1988), peripheral somatosensory receptors in humans (Gavrilov et al., 1976), cat spinal cord (Shealy and Henneman, 1962), and rodent hippocampal slices (Bachtold et al., 1998; Rinaldi et al., 1991). While these prior studies support the general potential of US for neurostimulation, high-intensity US can readily produce mechanical and/or thermal tissue damage (Dalecki, 2004; Hynynen and Clement, 2007; O'Brien, 2007; ter Haar, 2007), precluding it from use in noninvasive brain-circuit stimulation. At acoustic intensities <500 mW/cm^2, pulsed US can produce mechanical bioeffects without producing thermal effects or tissue damage (Dalecki, 2004; Dinno et al., 1989; O'Brien, 2007; ter Haar, 2007). In hippocampal slices, we previously reported low-intensity US (<300 mW/cm^2), low-frequency US (<0.65 MHz) is capable of stimulating action potentials and synaptic transmission (Tyler et al., 2008). Since low-frequency US can be reliably transmitted through skull bone (Hynynen and Clement, 2007; Hynynen et al., 2004), the motivation for the present study was to investigate the influence of low-frequency, low-intensity transcranial pulsed US on intact brain circuits in pursuit of a novel brain-stimulation method. We report that transcranial US is capable of safely and reliably stimulating in vivo brain circuits, such as the motor cortex and intact hippocampus of mice.

RESULTS

Construction and Transmission of Pulsed Ultrasound Stimulus Waveforms into Intact Brain Circuits

We constructed US stimulus waveforms and transmitted them into the intact brains of anesthetized mice (n = 192; Figure 1A). The optimal gains between transcranial transmission and brain absorption occurs for US at acoustic frequencies (f) $\leq$ 0.65 MHz (Hayner and Hynynen, 2001; White et al., 2006). Thus, we constructed transcranial stimulus waveforms with US having f = 0.25–0.50 MHz. Intensity characteristics of US stimulus waveforms were calculated based on industry standards and published equations developed by the American Institute of Ultrasound Medicine, the National Electronics Manufacturers Association, and the United Stated Food and Drug Administration (NEMA, 2004; see Experimental Procedures).

Single US pulses contained between 80 and 225 acoustic cycles per pulse (c/p) for pulse durations (PD) lasting 0.16–0.57 ms. Single US Pulses were repeated at pulse repetition frequencies (PRF) ranging from 1.2 to 3.0 kHz to produce spatial-peak temporal-average intensities (I_{SPTA}) of 21–163 mW/cm^2 for total stimulus duration ranging between 26 and 333 ms. Pulsed US waveforms had peak rarefactional pressures (p_r) of 0.070–0.097 MPa, pulse intensity integrals (PII) of 0.017–0.095 mJ/cm^2, and spatial-peak pulse-average intensities (I_{SPPA}) of 0.075–0.229 W/cm^2. Figures 1A, 1B, S1, and S2 illustrate the strategy developed for stimulating intact brain circuits with transcranial pulsed US. The attenuation of US due to propagation through the hair, skin, skull, and dura of mice was <10% (Figure 1C), and all intensity values reported were calculated from US pressure measurements acquired using a calibrated hydrophone positioned with a micromanipulator inside fresh ex vivo mouse heads at locations corresponding to the brain circuit being targeted.

Functional Stimulation of Intact Brain Circuits Using Pulsed Ultrasound

We first studied the influence of pulsed US on intact motor cortex because it enables electrophysiological and behavioral measures of brain activation (Movie S1). We recorded local field potentials (LFP) and multiunit activity (MUA) in primary motor cortex (M1) while transmitting pulsed US (0.35 MHz, 80 c/p, 1.5 kHz PRF, 100 pulses) having an I_{SPTA} = 36.20 mW/cm^2 through acoustic collimators (d = 4.7 mm) to the recording locations in anesthetized mice (n = 8; Figures 2A and 2B). Pulsed US triggered an LFP in M1 with a mean amplitude of -350.59 ± 43.34 μV (Figure 2B, 25 trials each). The LFP was associated with an increase in the frequency of cortical spikes (Figures 2C and 2D). This increase in spiking evoked by pulsed US was temporally precise and apparent within 50 ms of stimulus onset (Figure 2D). We found a broad range of pulsed US waveforms were equally capable of stimulating intact brain circuits as discussed below. Application of TTX (100 μM) to M1 (n = 4 mice) attenuated US-evoked increases in cortical activity, indicating that transcranial US stimulates neuronal activity mediated by action potentials (Figure 2B). These data provide evidence that pulsed US can be used to directly stimulate neuronal activity and action potentials in intact brain circuits.

We next acquired fine-wire electromyograms (EMG) and videos of muscle contractions in response to US stimulation of motor cortex in skin- and skull-intact, anesthetized mice (Movie S1). Using transcranial US to stimulate motor cortex, we evoked muscle contraction and movements in 92% of the mice tested. The muscle activity triggered by US stimulation of motor cortex produced EMG responses similar to those acquired during spontaneous muscle twitches (Figure 3A).

When using transducers directly coupled to the skin of mice, bilateral stimulation with transcranial US produced the near-simultaneous activation of several muscle groups, indicated by tail, forepaw, and whisker movements (Movie S2). By using acoustic collimators having an output aperture of d = 2.0, 3.0, or 4.7 mm and by making small ($\approx$2 mm) adjustments to the positioning of transducers or collimators over motor cortex within a subject, we could differentially evoke the activity of isolated muscle groups (Movie S2). Despite these intriguing observations, we found it difficult to reliably generate fine maps of mouse motor cortex using US for brain stimulation. The likeliest explanation for this difficulty is that the topographical/spatial segregation of different motor areas represented on the mouse cortex are below the resolution limits of US (see *Spatial Resolution of Brain Circuit Activation with Transcranial Pulsed Ultrasound* below).

The Influence of US Brain Stimulation Parameters on Motor Circuit Response Properties

When bilaterally targeted to motor cortex, pulsed US (0.50 MHz, 100 cycles per pulse, 1.5 kHz PRF, 80 pulses) having an I_{SPTA} = 64.53 mW/cm^2 triggered tail twitches and EMG activity in the lumbosacrocaudalis dorsalis lateralis muscle with a mean

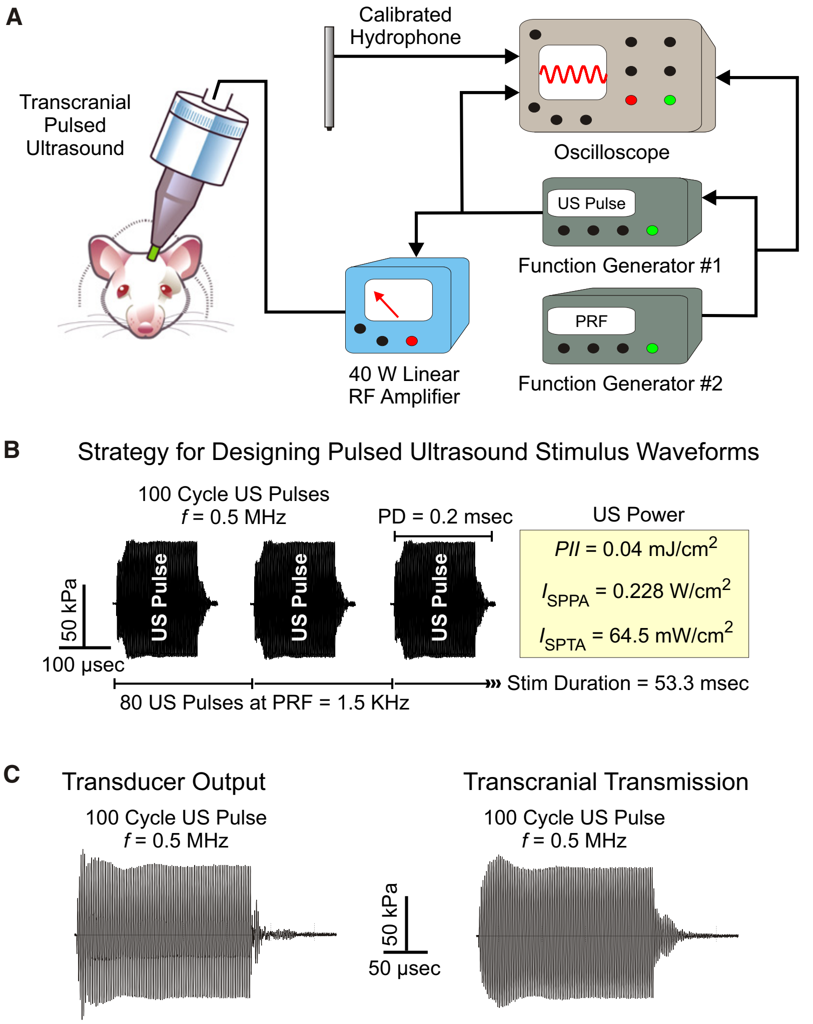
A
Calibrated Hydrophone
Transcranial Pulsed Ultrasound
Oscilloscope
US Pulse
Function Generator #1
PRF
Function Generator #2
40 W Linear RF Amplifier
B
Strategy for Designing Pulsed Ultrasound Stimulus Waveforms
100 Cycle US Pulses
f = 0.5 MHz
PD = 0.2 msec
US Power
PII = 0.04 mJ/cm2
ISPPA = 0.228 W/cm2
ISPTA = 64.5 mW/cm2
50 kPa
100 µsec
US Pulse
US Pulse
US Pulse
Stim Duration = 53.3 msec
80 US Pulses at PRF = 1.5 KHz
C
Transducer Output
100 Cycle US Pulse
f = 0.5 MHz
Transcranial Transmission
100 Cycle US Pulse
f = 0.5 MHz
50 kPa
50 µsec

Figure 1. Construction and Characterization of Low-Intensity Ultrasound Stimulus Waveforms for the Transcranial Stimulation of Intact Brain Circuits

(A) Illustration of the method used to construct and transmit pulsed US waveforms into the intact mouse brain. Two function generators were connected in series and used to construct stimulus waveforms. An RF amplifier was then used to provide final voltages to US transducers (see Figures S1 and S2 and Experimental Procedures).

(B) An example low-intensity US stimulus waveform is illustrated to highlight the parameters used in their construction. The acoustic intensities generated by the illustrated stimulus waveform are shown in the yellow box.

(C) Projected from a transducer surface to the face of a calibrated hydrophone, the acoustic pressure generated by a 100 cycle pulse of 0.5 MHz ultrasound is shown (left). The pressure generated by the same US pulse when transmitted from the face of the transducer through a fresh ex vivo mouse head to regions corresponding to motor cortex (0.8 mm deep) is shown (right).

response latency of 22.65 ± 1.70 ms (n = 26 mice). When unilaterally transmitted to targeted regions of motor cortex using a collimator (d = 3 mm), pulsed US (0.35 MHz, 80 c/p, 2.5 kHz PRF, 150 pulses) having an I_{SPTA} = 42.90 mW/cm^2 triggered an EMG response in the contralateral triceps brachii muscle with a mean response with latency of 20.88 ± 1.46 ms (n = 17 mice). With nearly identical response latencies (21.29 ± 1.58 ms), activation of the ipsilateral triceps brachii was also observed in ~70% of these unilateral stimulation cases (Movie S2). Although consistent from trial to trial (Figure 3B), the EMG response latencies produced by US brain stimulation were ≈10 ms slower than those obtained using optogenetic methods and intracranial electrodes to stimulate motor cortex (Ayling et al., 2009). Several reports show that TMS also produces response latencies slower than those obtained with intracranial electrodes (Barker, 1999). Discrepancies among the response latencies observed between electrical and US methods of brain stimulation are possibly due to differences in the time-varying energy profiles that these methods impart on brain circuits. The underlying core mechanisms of action responsible for mediating each brain-stimulation method are additional factors likely to influence the different response times.

The baseline failure rate in obtaining US-evoked motor responses was <5% when multiple stimulus trials were repeated once every 4–10 s for time periods up to 50 min (Figure 3B). As observed for response latencies in acute experiments, the peak amplitudes of EMG responses evoked by transcranial pulsed US were stable across trial number (Figure 3B). In more chronic situations, we performed repeated US stimulation experiments within individual subjects (n = 5 mice) on days 0, 7, and 14 using a trial repetition frequency of 0.1 Hz for 12–15 min each day. In these experiments, there were no differences in the peak amplitudes of the US-evoked EMG responses across days (day 0 mean peak EMG amplitude = 40.26 ± 0.99 µV, day 7 = 43.06 ± 1.52 µV, day 14 = 42.50 ± 1.42 µV; ANOVA $F_{2,\ 1303}$ = 1.47, p = 0.23; Figure S4A). These data demonstrate the ability of transcranial US to successfully stimulate brain circuit activity across multiple time periods spanning minutes (Figure 3B) to weeks (Figure S4A).

By examining EMG failure rates in eight mice, we next studied how the success of achieving motor activation was affected when stimulus trials were repeated in more rapid succession. The mean EMG failure probability significantly increased ($p < 0.001$) as the rate of US stimulus delivery increased from 0.25 to 5 Hz (Figure 3C and Movie S3). These data suggest that brain stimulation with US may not be useful at stimulation frequencies above 5 Hz. To confirm these observations and further explore this potential limitation, future investigations of an expanded US stimulus waveform space are required because it is not known how other US waveform profiles will influence the generation of sustained activity patterns.

We observed that application of TTX to motor cortex blocked EMG activity, which indicates that pulsed US triggers cortical

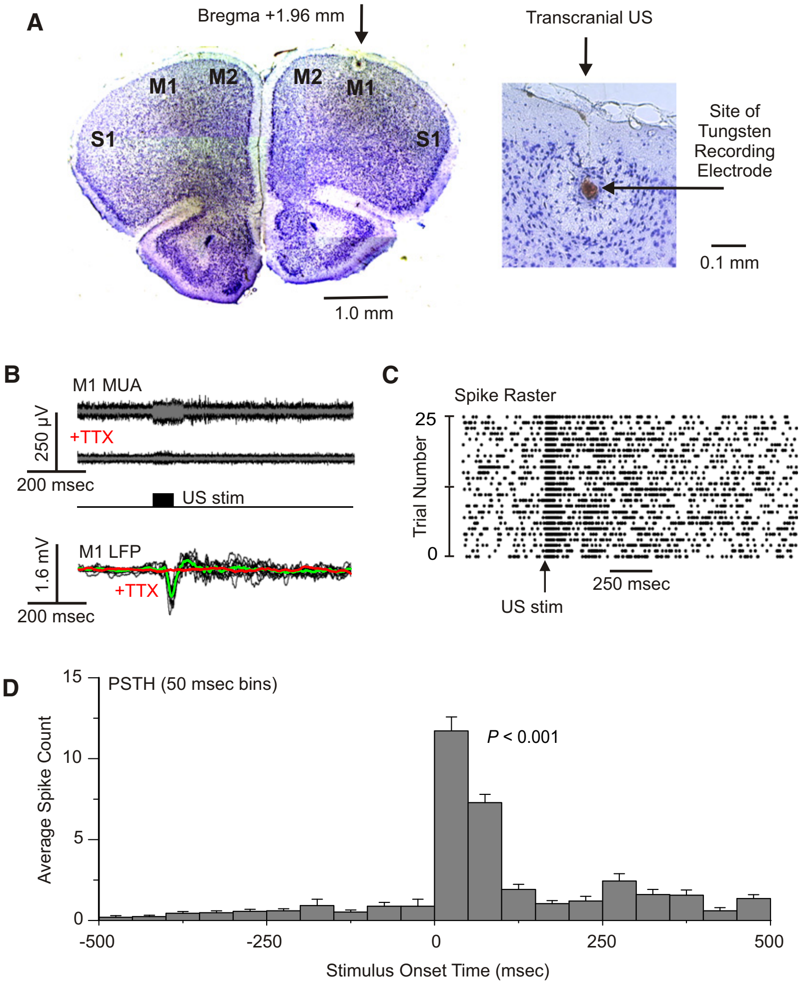

Figure 2. Low-Intensity Pulsed US Stimulates Neuronal Activity in the Intact Mouse Motor Cortex

(A) The coronal brain section shows an electrolytic lesion illustrating a recording site from which US-evoked neuronal activity was acquired in M1.

(B) (Top) Raw (black) and average (gray; 25 trials) US-evoked MUA recorded from M1 cortex in response to the delivery of pulsed US waveforms (Movie S1). (Middle) Addition of TTX to the cortex reduced synaptic noise and attenuated US-evoked MUA. (Bottom) Raw control (black), average control (green), and average TTX (red) LFP recorded from M1 cortex in response to 25 US stimulus waveforms delivered every 10 s.

(C) The spike raster plot illustrates the increase of cortical spiking as a function of time in response to 25 consecutive US stimulation trials.

(D) A poststimulus time histogram illustrates the average MUA spike count recorded 500 ms prior to and 500 ms following the delivery of US stimulus waveforms to motor cortex. Data shown are mean ± SEM.

action potentials to drive peripheral muscle contractions (n = 4 mice; Figure 3D). The intensities of US stimuli we studied were <500 mW/cm^2, where mechanical bioeffects have been well documented in the absence of thermal effects (Dalecki, 2004; Dinno et al., 1989; O'Brien, 2007; ter Haar, 2007). To confirm these observations in brain tissue, we monitored the temperature of motor cortex in response to US waveforms having different pulse duration (PD) times. Equations for estimating thermal absorption of US in biological tissues indicate that PD times are a critical factor for heat generation (O'Brien, 2007) and predict that 0.5 MHz US pulses exerting a p_r of 0.097 MPa for a PD of 0.57 ms should produce a temperature increase of 2.8×10^{-6} °C in brain (see Experimental Procedures). All US stimulus waveforms used in this study had p_r values <0.097 MPa and PD times $\leq$0.57 ms. None of the US waveforms used to stimulate cortex elicited a significant change in cortical temperature within our 0.01°C resolution limits (Figure 3E). We found that US pulses with p_r values of 0.1 MPa and PD times >50 ms were required to produce a nominal temperature change (ΔT) of 0.02°C (Figure 3E).

We next examined how acoustic frequencies and intensities across the ranges studied here influenced US-evoked EMG responses from the triceps brachii of mice (n = 20). We stimulated motor cortex using 20 distinct pulsed US waveforms composed with different US frequencies (0.25, 0.35, 0.425, and 0.5 MHz) and having varied intensities (Table S1). We randomized the sequence of which different waveforms were used in individual stimulus trials to avoid order effects. Relative comparisons of EMG amplitudes across animals can be influenced by many factors, including electrode placement, number of fibers recorded from, variation in noise levels, and differential fiber recruitment, which can be handled using normalization techniques to reduce intersubject variability (Kamen and Caldwell, 1996; Yang and Winter, 1984). To examine US-evoked EMG responses having the same dynamic range across animals, we normalized the peak amplitude of individual EMG responses to the maximum-peak amplitude EMG obtained for an animal and forced its minimum-peak amplitude EMG response through zero. A two-way ANOVA revealed a significant main effect of US frequency on EMG amplitude, where lower frequencies produced more robust EMG responses ($F_{3,\ 1085} = 3.95$, $p < 0.01$; Figure 4A). The two-way ANOVA also revealed a significant main effect of intensity (I_{SPTA}) on EMG amplitudes ($F_{19,\ 1085} = 9.78$, $p < 0.001$; Figure 4B), indicating that lower intensities triggered more robust EMG responses. The two-way ANOVA also revealed a significant frequency × intensity interaction ($F_{3,\ 1085} = 7.25$, $p < 0.01$; Figure 4C), indicating differential effects of US waveforms on neuronal activity as a function of frequency and intensity. Across the stimulus waveforms studied, we found that the EMG response latencies were not affected by either frequency or intensity (data not shown).

Spatial Distribution of Brain Circuit Activation with Transcranial Pulsed Ultrasound

To characterize the spatial distribution of US-evoked activity, we constructed functional activity maps using antibodies against

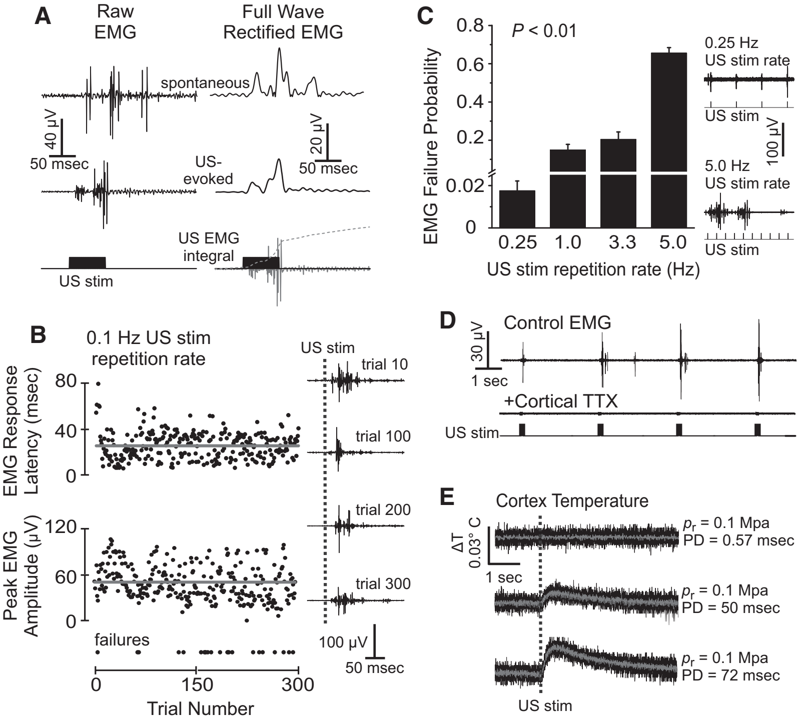

Figure 3. Transcranial Stimulation of Motor Cortex with Pulsed US Functionally Activates Descending Corticospinal Motor Circuits in Intact Mice

(A) Raw (left) and full-wave rectified (FWR; right) EMG traces obtained for a spontaneous muscle twitch (top) and average (ten trials) increase in muscle activity produced by transcranial US stimulation of motor cortex (bottom; Movie S1). The duration of the US stimulus waveform (black), average US-evoked EMG trace (gray), and EMG integral (gray dashed line) are shown superimposed at lower right.

(B) EMG response latencies (top) and amplitudes (bottom) recorded from the left triceps brachii in response to right motor cortex stimulation are plotted as a function of trial number repeated at 0.1 Hz. Individual US-evoked raw EMG traces are shown for different trials (right).

(C) EMG failure probability histograms are shown for four progressively increasing stimulus repetition frequencies (left; Movie S3). Raw US-evoked EMG traces are shown for two different stimulus repetition frequencies (right). Data shown are mean ± SEM.

(D) Raw EMG traces illustrating application of TTX to the motor cortex blocks US-evoked descending corticospinal circuit activity.

(E) Raw (black) and averaged (gray; ten trials) temperature recordings obtained from motor cortex in response to transmission of US waveforms with short pulse durations (PD) used in stimulus waveforms (top). Similarly, temperature recordings of cortex in response to waveforms having a PD ~100 times longer than those used in stimulus waveforms (middle and bottom).

c-fos (n = 4 mice). To facilitate data interpretation, we chose to stimulate intact brain tissue having a relatively planar surface and prominent subcortical structures. We centered the output of acoustic collimators (d = 2 mm; Figure S2C) over the skull covering the right hemisphere from −1.2 mm to −3.2 mm of Bregma and 0.5 mm to 2.5 mm lateral of the midline using stereotactic coordinates (Figure 5A; Franklin and Paxinos, 2007). We used our smallest-diameter collimator to characterize the minimal resolution of our brain-stimulation method since it is expected that larger collimators will produce larger areas of brain activation. Pulsed US (0.35 MHz, 50 c/p, 1.5 kHz PRF, 500 pulses) having an I_{SPTA} = 36.20 mW/cm^2 was transmitted along a vertical axis parallel to the sagittal plane through underlying brain regions once every 2 s for 30 min. Following a 45 min recovery period, mice were sacrificed and their brains were harvested for histology.

We prepared coronal sections from brain regions spanning +0.25 mm to −4.20 mm of Bregma (Figure 5A). Individual sections spaced every 125 µm were then immunolabeled using antibodies against c-fos and imaged using transmitted light microscopy. We quantified c-fos$^+$ cell densities in 250 × 250 µm squares for entire coronal sections, corrected for tissue shrinkage, and developed brain activity maps by plotting c-fos$^+$ cell densities in 250 × 250 µm pixels onto their corresponding anatomical locations using mouse brain atlas plates (Franklin and Paxinos, 2007). Representative raw data and functional activity maps coding c-fos$^+$ cell density using a psuedocolor lookup table for visualization purposes are shown in Figures 5B–5D. We estimated the lateral resolution of pulsed US along the rostral-caudal brain axis by analyzing regions of dorsal cortex (0.25–1.0 mm deep; 0.75–1.50 mm lateral of the midline) for each coronal section (Figures 5A–5D). An ANOVA comparing the mean c-fos$^+$ cell densities for each 250 × 250 µm square region collapsed across animals revealed that pulsed US produced a significant increase in the density of c-fos$^+$ cells (ANOVA, $F_{1,\ 646}$ = 73.39, $p < 0.001$; contralateral control hemisphere mean c-fos$^+$ cell density = 16.29 ± 0.20 cells/6.25 × 10^{-2} mm^2 compared to US stim = 19.82 ± 0.36 cells/6.25 × 10^{-2} mm^2). Subsequent pairwise comparisons of stimulated versus contralateral control cortex revealed that US stimulation produced a significant increase in c-fos$^+$ cell densities for a 1.5 mm region along the rostral-caudal axis (−1.38 mm to −2.88 mm of Bregma) under the 2.0 mm diameter stimulation zone (Figure 5E). Similar analyses along the medial-lateral axis of dorsal cortex revealed a significant increase ($p < 0.05$) in c-fos$^+$ cell densities for a 2.0 mm wide region of brain tissue under the stimulation zone (Figure S3B). We observed a smearing of elevated c-fos$^+$ cell densities lateral to the stimulation zone, which could be attributed to nonlinearities in our acoustic collimators (Figure S2C), the corticocortical lateral spread of activity, and/or slight lateral variations in the positioning of our collimators.

By examining the effects of pulsed US along the dorsal-ventral axis within the stimulation zone (0.5–2.5 mm medial to lateral; −1.2 to −3.2 mm of Bregma), we found the density of c-fos$^+$ cells was significantly higher ($p < 0.05$) compared to contralateral controls in the superficial 1.0 mm of tissue (Figure S3C). While there were trends of higher c-fos$^+$ cell densities in some deeper nuclei of stimulated hemispheres, we only observed one significant difference in a deep-brain

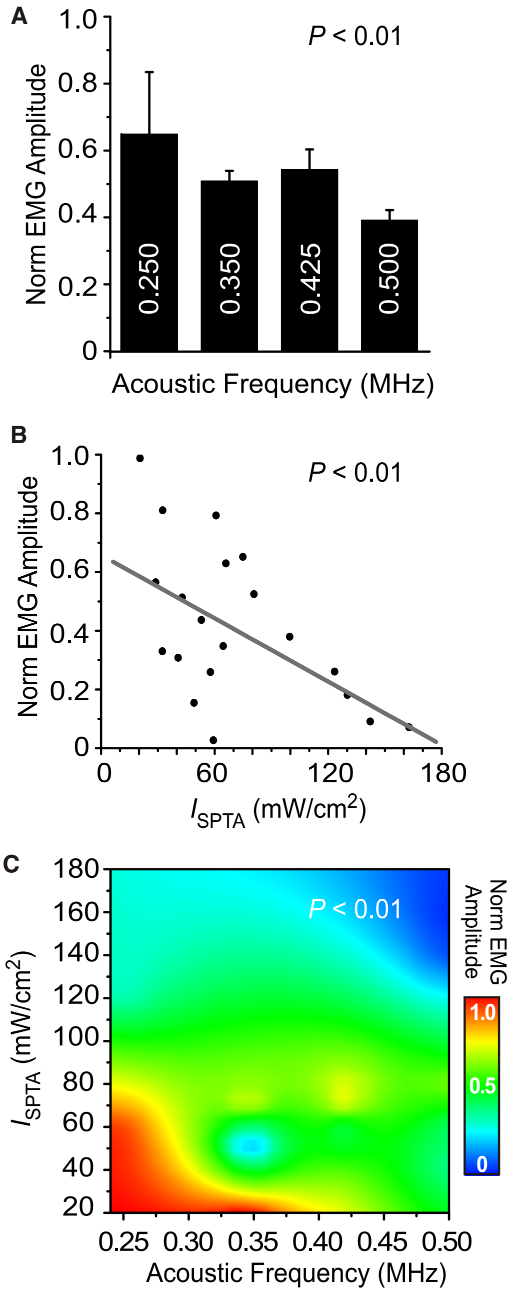

Figure 4. Interactions of the Acoustic Frequency and Acoustic Intensity of Stimulus Waveforms on Descending Corticospinal Circuit Activation

(A) Maximum-peak normalized (Norm) US-evoked EMG amplitude histograms are plotted for the four US frequencies used in the construction of stimulus waveforms. Data shown are mean ± SEM.

(B) Mean maximum-peak normalized US-evoked EMG amplitudes are plotted as a function of US intensities (I_{SPTA}) produced by 20 distinct stimulus waveforms (see Table S1).

(C) The interaction between US intensity (I_{SPTA}) and US frequency is plotted as a function of maximum-peak normalized EMG amplitudes (pseudocolor LUT).

region (Figure S3C). The elevated c-fos here may have been produced by standing waves or reflections, since higher c-fos$^+$ cell densities were generally observed near the skull base. Otherwise, we would have expected to observe elevated c-fos$^+$ levels uniformly along the dorsal-ventral axis of stimulated regions due to the transmission/absorption properties of US in brain tissue. For >1.5 mm of the 2.0 mm diameter cortical area we targeted with US in these mapping studies, regions deeper than $\approx$1 mm were ventral to dense white matter tracts (corpus callosum) in the brain. Interestingly, unmyelinated C-fibers have been shown to be more sensitive to US than myelinated Aδ fibers (Young and Henneman, 1961). Effectively blocking US-evoked activity in subcortical regions, we suspect low-intensity US fields may have been absorbed/scattered by dense white matter tracts in these mapping studies as a function of the US transmission path implemented. Despite these observations, we show below that it is indeed possible to stimulate subcortical brain regions with transcranial US by employing different targeting approaches (see *Remote Stimulation of the Intact Hippocampus Using Transcranial Pulsed US*).

Brain Stimulation with Low-intensity Transcranial Pulsed Ultrasound Is Safe in Mice

To assess the safety of transcranial US brain stimulation in mice, we first examined how pulsed US influenced blood-brain barrier (BBB) integrity. Prior to stimulation, mice received an intravenous administration of fluorescein isothiocyanate-dextran (10 kDa), which does not cross the BBB under normal conditions (Kleinfeld et al., 1998). The motor cortex of mice (n = 5) was then unilaterally stimulated every 10 s for 30 min with pulsed US (0.50 MHz, 225 cycles per pulse, 1.5 kHz PRF, 100 pulses) having an I_{SPTA} = 142.20 mW/cm^2 using a collimator (d = 4.7 mm). We observed no evidence that US produced damage to the BBB, as indicated by a complete lack of fluorescein leakage (contralateral control = 179.6 mm vasculature length examined versus US Stim = 183.4 mm vasculature length examined; Figure 6A). In separate positive control experiments, we coadministered intravenous fluorescein-dextran with an US contrast agent (Optison) shown to mediate in vivo BBB disruption in response to US (Raymond et al., 2008). Results from these positive control experiments (n = 3 mice) confirmed our ability to detect BBB damage had it occurred in response to pulsed US alone (Figure 6B).

We next probed the cellular-level consequences of pulsed US on brain tissues using antibodies against cleaved caspase-3 to monitor cell death (Figure 6C). Using the same US waveform described above (I_{SPTA} = 142.2 mW/cm^2), we unilaterally stimulated the motor cortex of mice (n = 8) every 10 s for 30 min. Following a 24 hr recovery period to allow for peak caspase-3 activation, mice were sacrificed and their brains examined using confocal microscopy. In comparing stimulated cortex regions with their contralateral controls (2.81 mm^2 total area/hemisphere/mouse), we found that pulsed US did not induce a change in the density of apoptotic glial cells (control = 0.40 ± 0.04 caspase-3$^+$ cells/0.56 mm^2 versus US Stim = 0.43 ± 0.06 caspase-3$^+$ cells/0.56 mm^2; p > 0.30) or apoptotic neurons (control = 0.08 ± 0.03 caspase-3$^+$ cells/0.56 mm^2 versus US stim = 0.07 ± 0.03 caspase-3$^+$ cells/0.56 mm^2; p > 0.50; Figure 6D). To further

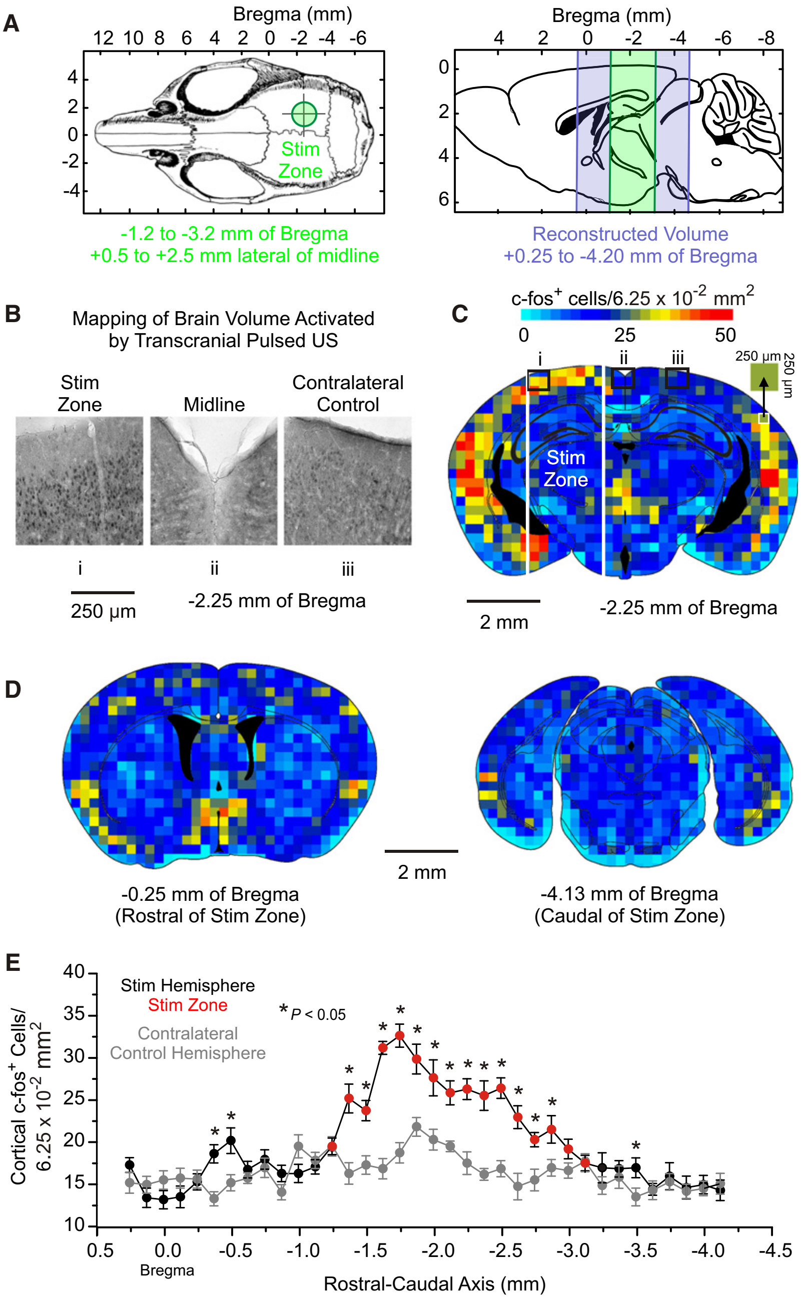

Figure 5. Spatial Distribution of Neuronal Activation Triggered by Transcranial Pulsed US

(A) Diagrams showing the anatomical locations where transcranial pulsed US was delivered through an acoustic collimator (green; d = 2 mm; Figure S2C) and the brain volume subsequently reconstructed (blue) to develop functional activity maps using antibodies against c-fos (Figure S3).

(B) Light micrographs showing c-fos activity in a coronal brain section at different locations inside (i) and outside (ii and iii) the US transmission path.

(C) A psuedocolored map of c-fos$^+$ cell densities in 250 × 250 μm regions is shown for a reconstructed coronal section obtained from within the stimulus zone. Small regions inside (i) and outside (ii and iii) the US brain transmission path are highlighted and contain c-fos density data obtained from the corresponding images shown in (B).

(D) Similar psuedocolored c-fos activity maps are shown for coronal brain sections rostral (left) and caudal (right) to the stimulated brain regions.

(E) The line plots illustrate the mean c-fos$^+$ cell densities observed along the rostral-caudal axis of reconstructed brain volumes for stimulated (black) and contralateral control hemispheres (gray). Regions of cortex within the stimulation zone are indicated in red. Data shown are mean ± SEM.

confirm this lack of an effect on cell death, we repeated the above experiment in mice (n = 4) using a higher-intensity US waveform (I_{SPTA} = 300 mW/cm^2), which is 137 mW/cm^2 higher intensity than we used to evoke brain activity with any waveform in this study. We again observed no significant effects (2.81 mm^2 total area/hemisphere/mouse) of pulsed US on the density of apoptotic glial cells (control = 0.44 ± 0.16 caspase-3$^+$ cells/0.56 mm^2 versus US stim = 0.38 ± 0.13 caspase-3$^+$ cells/0.56 mm^2; p > 0.30) or apoptotic neurons (control = 0.06 ± 0.05 caspase-3$^+$ cells/0.56 mm^2 versus US stim = 0.07 ± 0.05 caspase-3$^+$ cells/0.56 mm^2; p > 0.50; Figure 6D).

To determine the effects of pulsed US on brain ultrastructure, we used quantitative transmission electron microscopy to examine stimulated and control brains. We compared excitatory synapses in the motor cortex from control unstimulated mice (n = 5 mice) with synapses in the stimulated regions of motor cortex from mice (n = 6) that underwent a US stimulus trial as described above (I_{SPTA} = 142.2 mW/cm^2) every 10 s for 30 min (Figure 6E). An independent samples t test revealed no significant difference in the density of synapses between groups (control = 16.59 ± 0.81 synapses/100 μm^2 from 2.3 mm^2 versus US stim = 22.99 ± 4.07 synapses/100 μm^2 from 4.2 mm^2; p > 0.10; Figure 6F). There were also no significant differences in the postsynaptic density (PSD) length (control = 0.225 ± 0.009 μm from 99 synapses versus US stim = 0.234 ± 0.009 μm from 130 synapses; p > 0.10), the area of presynaptic terminals (control = 0.279 ± 0.02 μm^2 versus US stim = 0.297 ± 0.02 μm^2; p > 0.10), the density of vesicles in presynaptic boutons (control = 206.89 ± 9.52 vesicles/μm^2 versus US stim = 209.85 ± 8.14 vesicles/μm^2; p > 0.10), or the number of docked vesicles (DV) occupying active zones (control = 21.71 ± 0.91 DV/μm versus US stim = 20.26 ± 0.61 DV/μm; p > 0.10) between treatment groups (Figure 6F). There were no qualitative differences in the ultrastructure of cortical neuropil between treatment groups (Figure S4B).

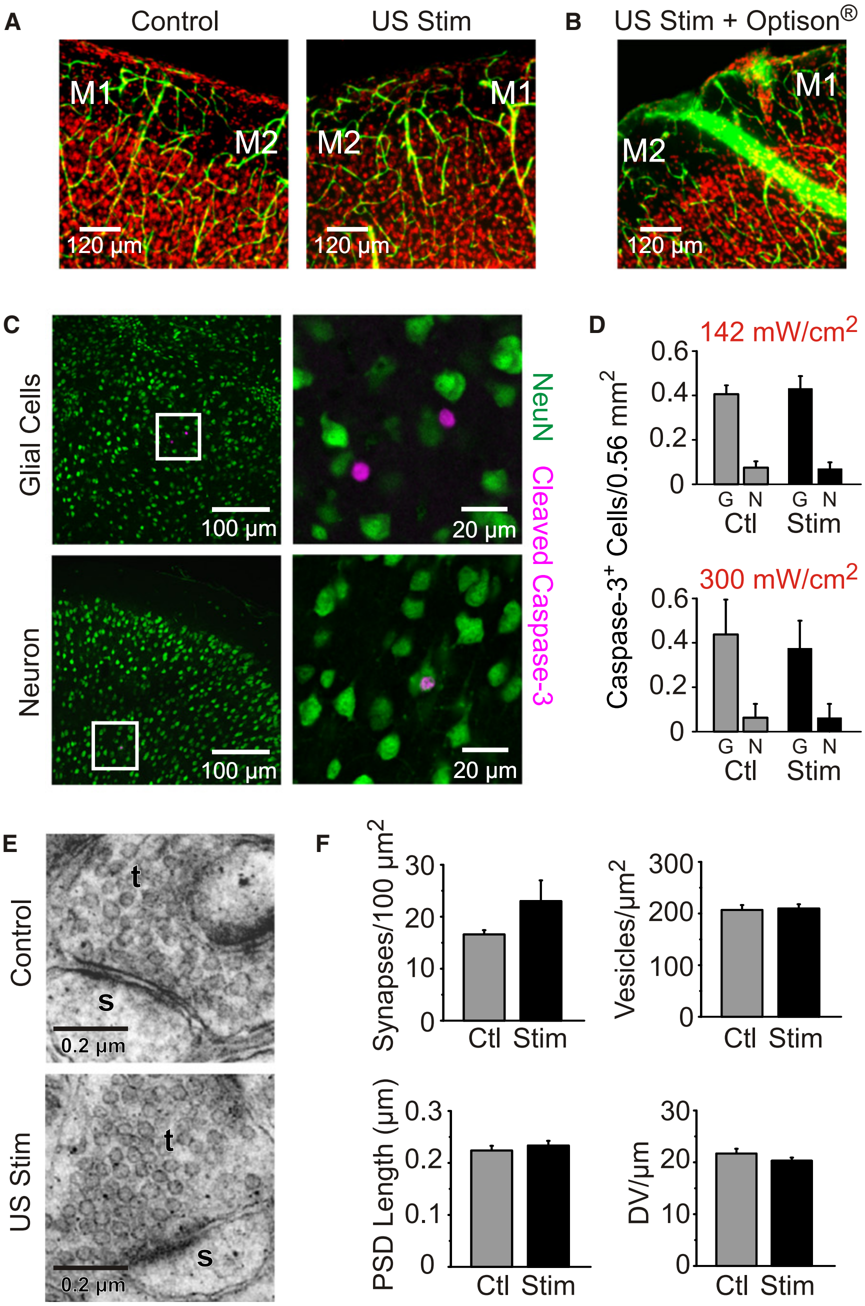

Figure 6. Transcranial Stimulation of Mouse Cortex with Low-Intensity Pulsed US Is Safe

(A) Confocal images of TO-PRO-3-labeled cells (red) and fluorescein-dextran-filled cerebrovasculature (green) obtained from the motor cortex of a contralateral control hemisphere (left) and from the stimulated region of the US-treated hemisphere (right).

(B) A similar confocal image is shown, but was obtained from a positive control treatment group where US-stimulation was performed in the presence of Optison, an ultrasound-microbubble contrast agent known to elicit cavitationally mediated vasculature damage.

(C) Confocal images of NeuN$^+$ (green) and cleaved caspase-3$^+$ (magenta) cells obtained from a US-stimulated region show positive glial cells (top) and a neuron (bottom) at low- (left) and high magnification (right).

(D) Histograms illustrate the mean density of cleaved caspase-3$^+$ glial cells ("G") and neurons ("N") observed in the motor cortex of contralateral control and US-stimulated hemispheres for two different stimulus intensity waveforms. Data shown are mean ± SEM.

(E) Transmission electron microscopic images (left) of excitatory synapses from control (top) and US-stimulated M1 cortex (bottom).

(F) Histograms are shown for mean synaptic density (top left), mean axonal bouton synaptic vesicle density (top right), mean PSD length (bottom left), and mean number of DV occupying active zones (bottom right).

Also see Figure S4.

To determine if transcranial US stimulation of motor cortex produced any gross impairments in motor behavior. The day before stimulation with pulsed US waveforms (I_{SPTA} = 142.2 mW/cm^2; every 10 s for 30 min), 24 hr poststimulation, and again 7 days poststimulation, we performed a series of experiments designed to assay motor function. Compared to sham-treated controls (n = 9 mice), a repeated-measures ANOVA revealed no significant effect of US stimulation (n = 9 mice) on a rotorod running task ($F_{1,8}$ = 0.211, p > 0.1; Figure S4C). We also measured motor function and grip strength by subjecting mice to a wire-hanging task. Again, repeated-measures ANOVA revealed no significant group effect on hang time ($F_{1,8}$ = 0.05; p > 0.1; Figure S4C). During daily behavioral monitoring, we observed no differences in feeding behavior, grooming behavior, or startle reflexes between US-stimulated mice and sham controls.

Through our development of the US brain-stimulation method described above, we have stimulated the intact brains of more than 190 mice through >92,000 US stimulus trails. We allowed >50% of the mice to recover from anesthesia following stimulation procedures and never observed any neurological abnormalities such as paralysis, ataxia, or tremor in these mice. Even mice undergoing multiple repeated-stimulation protocols spanning a 2 week time period (Figure S4A) exhibited no visible behavioral impairments or signs of diminishing responsiveness to transcranial pulsed US. In our studies, fewer than 6% of the animals died during or immediately following a US stimulation experiment. This mortality rate was likely due to respiratory or cardiac complications associated with maintaining mice under ketamine/xylazine anesthesia for extended periods of time (>2 hr). Based on the collective observations described above, we conclude that low-intensity transcranial pulsed US provides a safe and noninvasive method of stimulating intact brain circuit activity in mice. Whether similar safety margins hold true for other animal species must be directly evaluated and remains undetermined.

Remote Stimulation of the Intact Mouse Hippocampus Using Transcranial Pulsed US

We finally aimed to determine if trancranial pulsed US can be used to stimulate subcortical brain circuits in intact mice. To address this issue, we focused our attention on the intact mouse hippocampus, since pulsed US waveforms have been shown to elicit action potentials and synaptic transmission in hippocampal slices (Tyler et al., 2008). We performed extracellular recordings of US-evoked activity in the CA1 stratum pyramidale (s.p.) cell body layer of dorsal hippocampus (n = 7 mice). Prompted by our observations regarding the potential disruption of US fields by dense white matter tracts, we implemented a targeting approach bypassing the dense white matter of the corpus callosum when transmitting pulsed US to the hippocampus.

We used an angled line of US transmission through the brain by positioning acoustic collimators 50° from a vertical axis along the sagittal plane. The output aperture of collimators (d = 2 mm) were unilaterally centered over -4.5 mm of Bregma and 1.5 mm lateral of the midline (Figure 7A). We used a 30° approach angle to drive tungsten microelectrodes to the CA1 s.p. region of hippocampus through cranial windows (d = 1.5 mm) centered approximately -1.0 mm of Bregma (Figure 7A). Pulsed US (0.25 MHz, 40 cycles per pulse, 2.0 kHz PRF, 650 pulses) having an $I_{\mathrm{SPTA}} = 84.32$ mW/cm^2 reliably triggered an initial LFP with a mean amplitude of -168.94 ± 0.04 μV (50 trials each) and a mean response latency of 123.24 ± 4.44 ms following stimulus onset (Figure 7B and S5). This initial LFP was followed by a period of after-discharge activity lasting <3 s (Figure 7B and S5). These short-lived after-discharges did not appear to reflect abnormal circuit activity as observed during epileptogenesis (Bragin et al., 1997; McNamara, 1994; Racine, 1972). In fact, hippocampal after-discharges lasting more than 10 s are indicative of seizure activity (Racine, 1972).

Pulsed US produced a significant ($p < 0.01$) increase in spike frequency lasting 1.73 ± 0.12 s (Figure 7B). Natural activity patterns in the CA1 region of hippocampus exhibit gamma (40–100 Hz), sharp-wave (SPW) "ripple" (160–200 Hz), and other frequency-band oscillations reflecting specific behavioral states of an animal (Bragin et al., 1995; Buzsáki, 1989, 1996; Buzsáki et al., 1992). Sharp-wave ripples ($\approx$20 ms oscillations at $\approx$200 Hz) in CA1 result from the synchronized bursting of small populations of CA1 pyramidal neurons (Buzsáki et al., 1992; Ylinen et al., 1995) and have recently been shown to underlie memory storage in behaving rodents (Girardeau et al., 2009; Nakashiba et al., 2009). On the other hand, the consequences of gamma oscillations in the CA1 region of the hippocampus are not as well understood but are believed to stem from the intrinsic oscillatory properties of inhibitory interneurons (Bragin et al., 1995; Buzsáki, 1996). By decomposing the frequency components of wideband (1–10,000 Hz) activity patterns evoked by pulsed US, we found that all after-discharges contained both gamma oscillations and SWP ripple oscillations lasting <3 s (Figure 7C and S5). These data demonstrate that pulsed US can stimulate intact mouse hippocampus while evoking synchronous activity patterns and network oscillations; hallmark features of intrinsic hippocampal circuitry.

We naturally questioned whether these effects were accompanied by the regulation of activity-mediated cellular molecular signaling cascades in the hippocampus. Brain-derived neurotrophic factor (BDNF) is one of the most potent neuromodulators of hippocampal plasticity, and its expression/secretion is known to be regulated by neuronal activity (Lessmann et al., 2003; Poo, 2001). We thus examined BDNF protein expression levels in the hippocampus following transcranial stimulation with pulsed US. Unilateral hippocampi of mice (n = 7) were targeted and stimulated with pulsed US (0.35 MHz, 50 cycles per pulse, 1.5 kHz PRF, 500 pulses) having an $I_{\mathrm{SPTA}} = 36.20$ mW/cm^2 every 2 s for 30 min. Following a 45 min recovery period, mice were sacrificed and their brains removed, sectioned, and immunolabeled with antibodies against BDNF. We observed that pulsed US induced a significant increase in the density of BDNF$^+$ puncta in CA1 s.p. (contralateral control = 149.64 ± 11.49 BDNF$^+$ puncta/7.5×10^{-2} mm^2 from 0.61 mm^2 CA1 region/mouse versus US stim = 221.50 ± 8.75 BDNF$^+$ puncta/7.5×10^{-2} mm^2 from 0.61 mm^2 CA1 region/mouse; t test, $p < 0.001$; Figure 7D). Similar significant increases were observed in the CA3 s.p. region (contralateral control = 206.20 ± 19.68 BDNF$^+$ puncta/7.5×10^{-2} mm^2 from 0.61 mm^2 CA3 region/mouse versus US stim = 324.82 ± 27.94 BDNF$^+$ puncta/7.5×10^{-2} mm^2 from 0.61 mm^2 CA3 region/mouse; t test, $p < 0.005$; Figure 7D). These data demonstrate that pulsed US can be used to remotely stimulate neuronal activity in the intact mouse hippocampus. Posing captivating potential for broad applications in neuroscience, the increased synchronous activity and elevated BDNF expression patterns produced by pulsed US lend support to our hypothesis that transcranial US can be used to promote endogenous brain plasticity.

DISCUSSION

To date, previous studies detailing the effects of US on neuronal activity have fallen short of providing methods for its practical implementation in stimulating intact brain function. Prior studies examined the effects of US on neuronal activity by presonicating nervous tissues with US before examining its consequence on electrically evoked activity. These studies indeed revealed how US differentially affects the amplitude and duration of compound action potentials/field potentials evoked with traditional stimulating electrodes (Bachtold et al., 1998; Mihran et al., 1990; Rinaldi et al., 1991; Tsui et al., 2005). In other words, previous studies showed that US is capable of modulating electrically evoked activity but not that it alone could stimulate neuronal activity. We have provided clear evidence that transcranial pulsed US can stimulate intact brain circuits without requiring exogenous factors or surgery.

Due to temperature increases <0.01°C in response to US stimulus waveforms (Figure 5D), we propose a predominantly nonthermal (mechanical) mechanism(s) of action. The nonthermal actions of US are best understood in terms of cavitation—for example, radiation force, acoustic streaming, shock waves, and strain (Dalecki, 2004; Leighton, 2007; O'Brien,

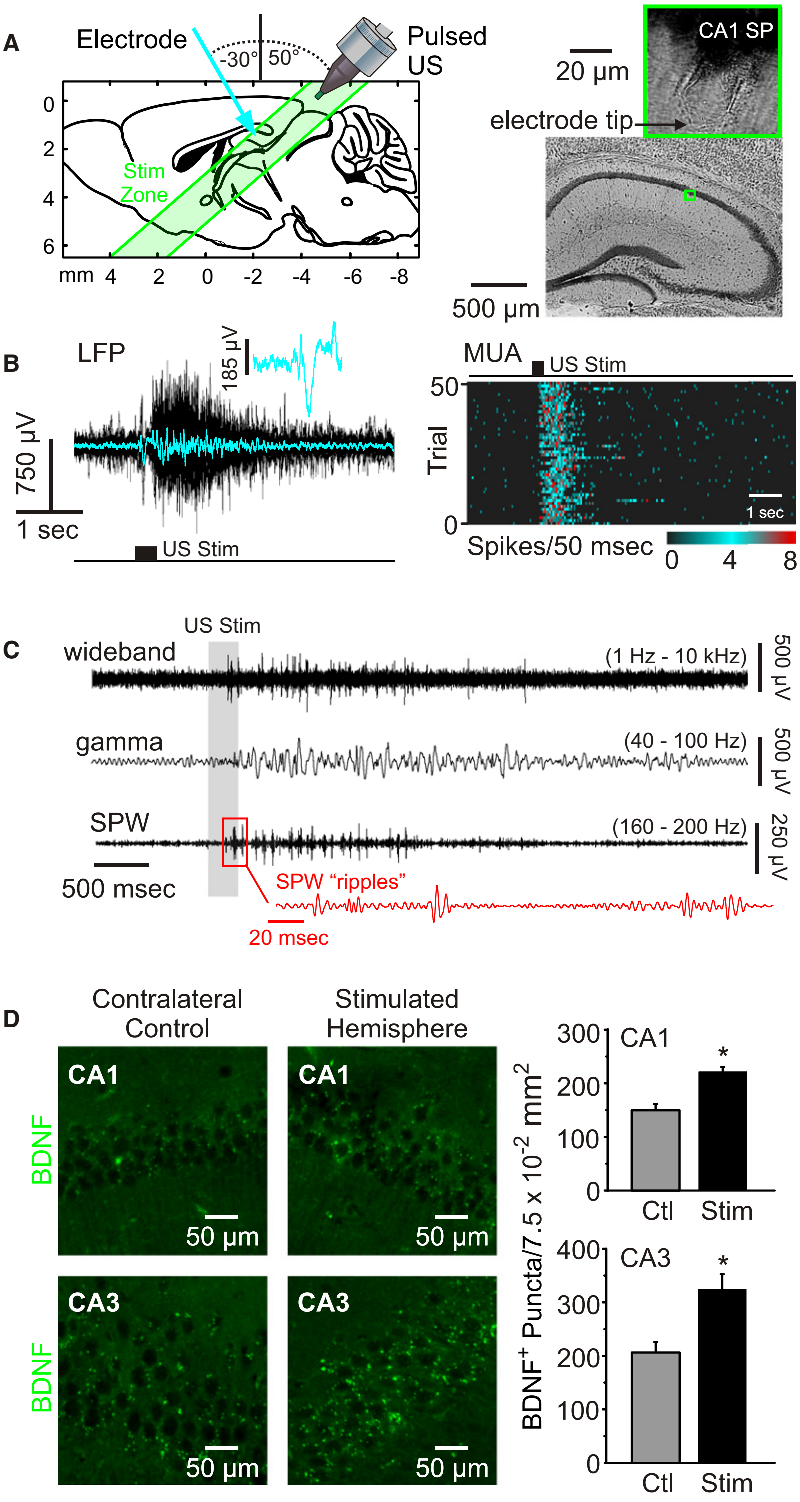

Figure 7. Transcranial Stimulation of the Intact Mouse Hippocampus with Pulsed Ultrasound

(A) Shown is an illustration of the geometrical configuration used for targeting the dorsolateral hippocampus with transcranial pulsed US while recording evoked electrophysiological responses in the dorsal hippocampus (left). A lesion illustrates the site of an electrophysiological recording location in the hippocampal CA1 s.p. region (right).

(B) Raw (black) and average (cyan) hippocampal CA1 LFP recorded in response to 50 consecutive US stimulation trials (left). A psuedocolored spike-density plot illustrates the increase in CA1 s.p. spiking as a function of time in response to 50 consecutive pulsed US stimuli delivered at 0.1 Hz (right).

(C) An individual recording trace of CA1 s.p. extracellular activity in response to a pulsed US waveform is shown in its wideband (top), gamma (middle), and SWP (bottom) frequency bands. An expanded 250 ms region of the SWP trace (red) illustrates SWP "ripples" (also see Figure S5).

(D) Confocal images illustrating BDNF (green) expression in the CA1 s.p. (top) and CA3 s.p. (bottom) regions of hippocampus from contralateral control (left) and stimulated hemispheres (right). Histograms (far right) illustrate the significant increase in the density of BDNF$^+$ puncta triggered by transcranial US stimulation for the CA1 s.p. (top) and CA3 s.p. (bottom) regions of hippocampus. Data shown are mean ± SEM.

2007). Accordingly, we have proposed a continuum mechanics hypothesis of ultrasonic neuromodulation, where US produces fluid-mechanical effects on the cellular environments of neurons to modulate their resting membrane potentials (Tyler, 2010). The direct activation of ion channels by US may also represent a mechanism of action, since many of the voltage-gated sodium, potassium, and calcium channels influencing neuronal excitability possess mechanically sensitive gating kinetics (Morris and Juranka, 2007). Pulsed US could also produce ephaptic effects or generate spatially inhomogeneous electric fields, proposed to underlie aspects of synchronous activity (Anastassiou et al., 2010; Jefferys and Haas, 1982). Clearly, further studies are required to dissect mechanisms underlying the ability of US to stimulate intact brain circuits.

Our observations also serve as preliminary evidence that pulsed US can be used to probe intrinsic characteristics of brain circuits. For example, US stimulation of motor cortex produced short bursts of activity (<100 ms) and peripheral muscle contractions, whereas stimulation of the hippocampus with similar waveforms triggered characteristic rhythmic bursting (recurrent activity), which lasted 2–3 s. These observations lead us to question whether stimulation of a given brain region with US can mediate even broader circuit activation based on functional connectivity. Such abilities have been shown and discussed for other transcranial brain-stimulation approaches like TMS (Huerta and Volpe, 2009). Future studies should be designed to study the influence of US on activity in corticothalamic, corticocortical, and thalamocortical pathways as we have done here for corticospinal circuits. Similar to widely recognized observations using other cortical-stimulation methods (Angel and Gratton, 1982; Goss-Sampson and Kriss, 1991), we found that the success of brain activation with transcranial pulsed US was dependent on the plane of anesthesia. When mice were in moderate to light anesthesia planes (mild responsiveness to tail pinch), we found that US-evoked activity was highly consistent across multiple repeated trials as described above.

Although our observations indicate that pulsed US provides a safe mode of brain stimulation in mice (Figure 6 and S4), it should not be inferred that the same is true for other animal species. Safety studies in other animals are required for any such conclusions to be drawn. Since we suspect that standing waves may inadvertently influence the activity of some brain regions under certain conditions, future studies should attend to the influence of such reflections on brain tissue, regardless of the focusing method implemented. This is particularly true for cases where high-intensity ultrasound may be used to treat brain tissues as discussed below. The less-direct safety implications of our study also need to be considered. Diagnostic fetal US has been shown to disrupt neuronal migration in developing rat fetal brains (Ang et al., 2006). Those effects could be due to the influence of US on neuronal activity or growth factor expression patterns in developing fetal brains. Having dire ramifications on the global use of diagnostic fetal ultrasound, investigations into such possibilities are warranted.

Using a method of transcranial US brain stimulation with an acoustic collimating tube (d = 2 mm; Figure S2C), we estimated the volume of cortical activation to be ≈ 3 mm^3 as indicated by c-fos activity (Figures 5 and S3). As previously discussed, however, this activated brain volume may have been restricted by anatomical features along the dorsal-ventral US transmission path we implemented (for example the corpus callosum restricting the depth of activation to the cortex) and needs to be further explored before more accurate conclusions regarding the axial resolution can be drawn. The 1.5–2.0 mm lateral area of activation we observed represents a more reliable measure and is approximately five times better than the ≈ 1 cm lateral spatial resolution offered by TMS (Barker, 1999). Due to the millimeter spatial resolutions conferred by US, it may be possible to use structured US fields to drive patterned activation in sparsely distributed brain circuits. Similarly, focusing with acoustic metamaterials (having a negative refractive index) enables subdiffraction spatial resolutions to be achieved for US (Zhang et al., 2009). Based on those findings, it is not unreasonable to expect that brain regions <1.0 mm may be accurately targeted for neurostimulation using 0.5 MHz US. Such spatial scales would indeed make transcranial US for brain stimulation amenable to a variety of research and clinical applications. With respect to the spatial resolutions of brain stimulation approaches, however, optogenetic approaches still reign superior when micron-scale resolutions are required—for example, in the fine functional mapping of intact mouse brain circuits (Ayling et al., 2009; Hira et al., 2009) or in the study of single-cell/single-synapse physiology (Zhang et al., 2007; Zhang et al., 2008).

Focusing of US through skull bones, including those of humans, can be achieved using transducers arranged in phased arrays (Hynynen et al., 2004; Hynynen et al., 2006; Martin et al., 2009). A recent clinical study reported using transcranial MRI-guided high-intensity focused ultrasound (0.65 MHz, >1000 W/cm^2) to perform noninvasive thalamotomies (d = 4.0 mm) for the treatment of chronic neuropathic pain by focusing US through the intact human skull to deep thalamic nuclei using phased arrays (Martin et al., 2009). These abilities to focus US through the intact skull into the deep-brain regions certainly raise the possibility of using pulsed US in the noninvasive stimulation of human brain circuits. However, cautiously conducted preclinical safety and efficacy studies are required across independent groups before it can be determined if pulsed US might be useful in such an application.

We recognize that several issues need further investigation before the potential of transcranial US for brain stimulation can be realized. However, it has not escaped our attention that transcranial pulsed US might serve as a foundation for radical new approaches to the study of brain function/dysfunction. For instance, since US is readily compatible with magnetic resonance imaging (MRI) it is feasible that pulsed US could be used for brain-circuit stimulation during simultaneous MRI imaging in the functional brain mapping of intact, normal or diseased brains. It is conceivable that pulsed US could be used to induce forms of endogenous brain plasticity as shown with TMS (Pascual-Leone et al., 1994). In such an embodiment, pulsed US might drive specific brain activity patterns shown to underlie certain cognitive processes like memory trace formation (Girardeau et al., 2009; Nakashiba et al., 2009). This particularly intriguing possibility is supported by our observations in mice that transcranial US can promote sharp-wave ripple oscillations (Figures 7C and S5) and stimulate the activity of endogenous BDNF (Figure 7D), an important regulator of brain plasticity and hippocampal-dependent memory consolidation (Tyler et al., 2002). Based on this study demonstrating that transcranial pulsed US is capable of stimulating intact brain circuits, one can begin to imagine a vast number of applications where this method might enable us to better understand and manipulate brain function.

EXPERIMENTAL PROCEDURES

Generation and Characterization of Pulsed US Waveforms

We used immersion-type US transducers having a center frequency of 0.5 MHz (V301-SU, Olympus NDT, Waltham, MA) or 0.3 MHz (GS-300-D19, Ultran, State College, PA) to produce US waveforms. US pulses were generated by brief bursts of square waves (0.2 μs; 0.5 mV peak-to-peak) using an Agilent 33220A function generator (Agilent Technologies, Inc., Santa Clara, CA, USA). Square waves were further amplified (50 dB gain) using a 40 W ENI 240L RF amplifier. Square waves were delivered between 0.25 and 0.50 MHz depending on the acoustic frequency desired. US pulses were repeated at a pulse repetition frequency by triggering the above-referenced function generator with square waves produced using a second Agilent 33220A function generator (Figure S1).

To characterize the intensity characteristics of pulsed US stimulus waveforms, we recorded voltage traces produced by US pressure waves using a calibrated needle hydrophone (HNR 500, Onda Corporation, Sunnyvale, CA, USA) and an Agilent DSO6012A 100 MHz digital oscilloscope connected to a PC. Intensity measurements were made from targeted points inside fresh ex vivo mouse heads corresponding to the brain region targeted. The transcranial US waveforms were transmitted to intact brain circuits from US transducers using custom-designed acoustic collimators consisting of 3.0 or 4.7 mm (1 ml syringe) diameter polyethylene tubing or 5.0 mm diameter tubing tapered to a 2.0 mm diameter output aperture (Figure S2C). Collimating guides were constructed so stimulated regions of the brain were in the far field of US transmission paths and filled with ultrasound coupling gel.

Using measurements recorded from calibrated hydrophones (described above), we calculated several acoustic intensity characteristics of pulsed US stimulus waveforms based on published and industry accepted standards (NEMA, 2004).

The pulse intensity integral (*PII*) was defined as

$$PII = \int \frac{p^2(t)}{Z_0} dt$$

where p is the instantaneous peak pressure, Z_0 is the characteristic acoustic impedance in Pa s/m defined as ρc where ρ is the density of the medium, and c is the speed of sound in the medium. We estimated ρ to be 1028 kg/m^3 and c to be 1515 m/s for brain tissue based on previous reports (Ludwig, 1950). The spatial-peak, pulse-average intensity (I_{SPPA}) was defined as

$$I_{\mathrm{SPPA}} = \frac{PII}{PD}$$

where PD is the pulse duration defined as $(t)(0.9PII - 0.1PII)\ 1.25$ as outlined by technical standards established by AIUM and NEMA (NEMA, 2004).

The spatial-peak temporal-average intensity (I_{SPTA}) was defined as $I_{SPTA} = PII(\mathrm{PRF})$, where PRF is equal to the pulse repetition frequency in hertz.

The mechanical index (MI; see Table S1) was defined as

$$\mathrm{MI} = \frac{p_r}{\sqrt{f}}$$

In Vivo US Stimulation

In this study, we used wild-type mice in accordance with animal-use protocols approved by the Institutional Animal Care and Use Committee at Arizona State University. To conduct transcranial US stimulation of intact motor cortex, mice were anesthetized using a ketamine-xylazine cocktail (70 mg/kg ketamine, 7 mg/kg xylazine) administered intraperitoneally. The hair on the dorsal surface of the head over regions corresponding to targeted brain regions was trimmed. Mice were then placed in a custom-designed or Cunningham mouse stereotax. US transducers with affixed collimators were lowered to points above the skin corresponding to brain regions using standard stereotactic coordinates. Collimators or transducers were then placed on the surface of the skin above the targeted brain region and coupled to the skin using ultrasound gel. Transcranial pulsed US stimulus waveforms were delivered to the targeted motor cortex or hippocampus using standard TTL triggering protocols (Figure S1). Digital signal markers indicated the onset and length of US stimulus waveforms. During some experiments, simultaneous electrophysiological data were acquired (see below). Only in experiments where we conducted in vivo extracellular recordings of brain activity or brain temperature was a craniotomy performed. Since cranial windows and electrode insertions were made at sites adjacent to angled US projection lines targeting specific brain regions, in these cases the US was still transmitted through skull bone, although not covered by overlying skin. All other experiments were conducted in wholly intact mice, except for some mapping experiments that required retraction of the skin to identify landmarks on the mouse skull. Following stimulation, animals were either allowed to recover from anesthesia or processed as described below.

Extracellular Recordings

Extracellular activity was recorded using standard approaches with tungsten microelectrodes (500 kΩ to 1 MΩ, FHC, Inc., Bowdoin, ME, USA). Tungsten microelectrodes were driven to recording sites through cranial windows (d = 1.5 mm) based on stereotactic coordinates and confirmed by electrophysiological signatures. Tungsten microelectrodes were connected to a Medusa PreAmp (RA16PA; Tucker-Davis Technologies, Aluchua, FL, USA) and a multichannel neurophysiology workstation (Tucker-Davis Technologies) or a 16 channel DataWave Experimenter and SciWorks (DataWave Technologies, Berthoud, CO) to acquire extracellular activity. Raw extracellular activity in response to pulsed US was acquired at a sampling frequency of 24.414 kHz in 10 s trial epochs. The MUA signal was resampled at 1.017 kHz and bandpass filtered between 0.3 to 6 kHz, the LFP signal was filtered between 1 and 120 Hz, wideband activity was filtered between 0.001 and 10 kHz, gamma band activity was filtered between 40 and 100 Hz, and the SWP ripple band was filtered between 160 and 200 Hz. Data analyses were subsequently performed offline.

EMG Recordings

Fine-wire EMG recordings were made using standard approaches and a four-channel differential AC amplifier (model 1700, A-M Systems, Inc., Sequim, WA, USA) with 10–1000 Hz band-pass filter and a 100× gain applied. Electrical interference was rejected using a 60 Hz notch filter. EMG signals were acquired at 2 kHz using a Digidata 1440A and pClamp or a 16 channel DataWave Experimenter and SciWorks. Briefly, small barbs were made in a 2 mm uncoated end of Teflon-coated steel wire (California Fine Wire, Co., Grover Beach, CA, USA). Single recording wires were then inserted into the appropriate muscles using a 30 gauge hypodermic syringe before being connected to the amplifier. Ground wires were similarly constructed and subcutaneously inserted into the dorsal surface of the neck.

Brain Temperature Recordings and Estimated Changes

Prior to US stimulation in some experiments, we performed a small craniotomy (d ≈ 2 mm) on mouse temporal bone. Following removal of dura, we inserted a 0.87 mm diameter thermocouple (TA-29, Warner Instruments, LLC, Hamden, CT, USA) into motor cortex through the cranial window. The thermocouple was connected to a monitoring device (TC-324B, Warner Instruments) and to a Digidata 1440A to record temperature (calibrated voltage signal = 100 mV/°C) using pClamp.

We also estimated the influence of US stimulus waveforms on brain temperature change using a set of previously described equations valid for short exposure times (O'Brien, 2007). Briefly, we estimated the maximum temperature change (ΔT_{max}) to be

$$\Delta t_{max} = \frac{\dot{Q}\Delta t}{C_v}$$

where Δt is the pulse exposure time, where C_{v} is the specific heat capacity for brain tissue ≈ 3.6 J/g/K (Cooper and Trezek, 1972), and where $\dot{Q}$ is the rate at which heat is produced defined by Nyborg (1981):

$$\dot{Q} = \frac{\alpha p_0^2}{\rho c}$$

where ρ is the density of the medium, c is the speed of sound in the medium as described above, where α is the absorption coefficient of brain (≈ 0.03 Np/cm for 0.5 MHz US; Goss et al., 1978), and p_0 is the pressure amplitude of US stimulus waveforms.

Transmission Electron Microscopy

Following stimulation, animals were transcardially perfused with 2% glutaraldehyde, 2.5% formaldehyde in sodium cacodylate buffer. Brains were subsequently removed and postfixed in 2% glutaraldehyde, 2.5% formaldehyde in sodium cacodylate buffer overnight in 4°C. Following postfixation and sodium cacodylate buffer rinsing, secondary fixation was performed with 0.2% osmium textroxide in sodium cacodylate for 1 hr. Sections were then block-stained overnight at 4°C with 0.25% uranyl acetate before being dehydrated in a graded ethanol series followed by 100% acetone. Samples were infiltrated Spur's resin during the next 3 days and flat embedded on Teflon-coated glass slides before being polymerized overnight at 60°C. Motor cortex regions of interest were then identified and trimmed prior to block mounting. Trimmed sections were then ultra-thin sectioned at 70 nm on an ultramicrotome (Leica Ultra Cut R, Leica Microsystems, Inc., Bannockburn, IL, USA). Samples were collected on formvar-coated copper slot grids and poststained with 1% uranyl acetate in ethanol and Sato's lead citrate. Samples were imaged at 80 kV on a Phillips CM12 transmission electron microscope and images acquired with a Gatan CCD camera (model 791, Gatan, Inc., Warrendale, PA, USA). Images were acquired at 8000× for analysis of overall ultrastructure, 19,500× for analysis of synaptic density, and 40,000× quantitative analysis of synapse-specific parameters.

Histological Evaluation

In some experiments, we performed histological investigations of stimulated and unstimulated brain regions of mice receiving transcranial US stimulation of motor cortex. To prepare tissue for histology, mice were transcardially perfused using 4% paraformaldehyde in PBS. Mouse brains were removed and postfixed in 4% paraformaldehyde at 4°C overnight. Coronal slices of stimulated and adjacent unstimulated motor cortex were then made using a vibratome or a cryotome. For mapping studies, coronal cryosections were immunolabeled using antibodies against c-fos (1:250; SC-253, Santa Cruz Biotechnology, Inc., Santa Cruz, CA, USA) and standard processing techniques with Vectastain Elite ABC kits (Vector Laboratories, Burlingame, CA) before being imaged using transmitted light microscopy. In other histological analyses, brain sections (50 μm) were double-labeled using standard immunocytochemistry techniques with antibodies against cleaved caspase-3 (1:250; Asp 175-9661, Cell Signaling Technology, Beverly, MA, USA), BDNF (1:1000, AB1534SP, Millipore, Billerica, MA), and/or NeuN (1:1000, MAB377, Millipore). Following overnight primary antibody incubation, sections were washed and incubated in appropriate Alexa Fluor 488, Alexa Fluor 568, or Alexa Fluor 633 secondary antibodies (1:500; Invitrogen, Carlsbad, CA, USA) for 2 hr at room temperature. One- or two-channel fluorescence images were acquired on an Olympus Fluoview FV-300 laser-scanning confocal microscope (Olympus America, Inc., Center Valley, PA, USA).

Prior to US-stimulation trials, some animals received an intravenous infusion of 5% fluorescein isothiocyanate-dextran (10 kDa; Sigma, St. Louis, MO, USA) in a 0.9% sodium chloride solution (0.35 mL). Coronal sections (75 μm) of these brains were prepared using a vibratome. Floating sections were then labeled with TO-PRO-3 (1:1000; Invitrogen) to identify cell bodies. Following washing and mounting, the cerebrovasculature was then examined using confocal microscopy. In additional positive control experiments, prior to US stimulation mice received an intravenous infusion of 5% fluorescein isothiocyanate-dextran in conjunction with an ultrasound contrast agent (Optison; GE Healthcare, Piscataway, NJ, USA) known to elicit BBB disruption during US administration (Raymond et al., 2008). These brains were processed and examined as described above.

Behavioral Assays

US-stimulated and sham-treated control mice were subjected to behavioral testing using a rotorod task and a wire-hanging task. On US stimulation treatment day, sham-treated controls and US-stimulated animals were anesthetized with ketamine/xylazine and their hair was trimmed. Following US stimulation or sham-treatment, motor skill testing was administered on rotorod and wire-hanging tasks again at 24 hr and 7 days later and compared against 24 hr prestimulation control performance. On behavioral testing days, mice ran on the rotorod (25.4 cm circumference, 10.8 cm wide rod) until failure (time in seconds before falling from rotorod) for five trials each at two speeds (17 and 26 RPM). Following rotorod trials, animals performed wire-hanging tests until failure time (time in seconds before falling from suspended wire) for five trials.

Data Analyses

All electrophysiological data (MUA, LFP, and EMG) were processed and analyzed using custom-written routines in Matlab (The Mathworks, Natick, MA, USA) or Clampfit (Molecular Devices). Single spikes were isolated using a standard thresholding window. Ultrasound waveform characteristics were analyzed using hydrophone voltage traces and custom-written routines in Matlab and Origin (OriginLab Corp., Northampton, MA, USA). All histological confocal and transmitted light images were processed and analyzed using *ImageJ* (http://rsb.info.nih.gov/ij/). Electron microscopy data were also quantified using *ImageJ*. All statistical analyses were performed using SPSS (SPSS, Inc., Chicago, IL, USA). Data shown are mean ± SEM unless indicated otherwise.

SUPPLEMENTAL INFORMATION

Supplemental Information includes five figures, one table, and three movies and can be found with this article online at doi:10.1016/j.neuron.2010.05.008.

ACKNOWLEDGMENTS

We thank Dr. William T. Newsome of Stanford University for his critical feedback and insightful discussions regarding this manuscript. We thank Joshua Nichols, Zachary Gilbert, and Erik Handberg for their assistance in performing some of the behavioral experiments. Funding for this research was provided by start-up funds from Arizona State University to W.J.T. and a Department of Defense grant to W.J.T. from the US Army Research, Development, and Engineering Command (RDECOMW911NF-09-0431). W.J.T. is the cofounder of SynSonix.

Accepted: April 29, 2010
Published: June 9, 2010

REFERENCES

Anastassiou, C.A., Montgomery, S.M., Barahona, M., Buzsáki, G., and Koch, C. (2010). The effect of spatially inhomogeneous extracellular electric fields on neurons. J. Neurosci. *30*, 1925–1936.

Ang, E.S., Jr., Gluncic, V., Duque, A., Schafer, M.E., and Rakic, P. (2006). Prenatal exposure to ultrasound waves impacts neuronal migration in mice. Proc. Natl. Acad. Sci. USA *103*, 12903–12910.

Angel, A., and Gratton, D.A. (1982). The effect of anaesthetic agents on cerebral cortical responses in the rat. Br. J. Pharmacol. *76*, 541–549.

Ayling, O.G., Harrison, T.C., Boyd, J.D., Goroshkov, A., and Murphy, T.H. (2009). Automated light-based mapping of motor cortex by photoactivation of channelrhodopsin-2 transgenic mice. Nat. Methods *6*, 219–224.

Bachtold, M.R., Rinaldi, P.C., Jones, J.P., Reines, F., and Price, L.R. (1998). Focused ultrasound modifications of neural circuit activity in a mammalian brain. Ultrasound Med. Biol. *24*, 557–565.

Barker, A.T. (1999). The history and basic principles of magnetic nerve stimulation. Electroencephalogr. Clin. Neurophysiol. Suppl. *51*, 3–21.

Bragin, A., Jandó, G., Nádasdy, Z., Hetke, J., Wise, K., and Buzsáki, G. (1995). Gamma (40-100 Hz) oscillation in the hippocampus of the behaving rat. J. Neurosci. *15*, 47–60.

Bragin, A., Penttonen, M., and Buzsáki, G. (1997). Termination of epileptic afterdischarge in the hippocampus. J. Neurosci. *17*, 2567–2579.

Buzsáki, G. (1989). Two-stage model of memory trace formation: a role for "noisy" brain states. Neuroscience *31*, 551–570.

Buzsáki, G. (1996). The hippocampo-neocortical dialogue. Cereb. Cortex *6*, 81–92.

Buzsáki, G., Horváth, Z., Urioste, R., Hetke, J., and Wise, K. (1992). High-frequency network oscillation in the hippocampus. Science *256*, 1025–1027.

Cooper, T.E., and Trezek, G.J. (1972). A probe technique for determining the thermal conductivity of tissue. J. Heat Transfer *94*, 130–140.

Dalecki, D. (2004). Mechanical bioeffects of ultrasound. Annu. Rev. Biomed. Eng. *6*, 229–248.

Dinno, M.A., Dyson, M., Young, S.R., Mortimer, A.J., Hart, J., and Crum, L.A. (1989). The significance of membrane changes in the safe and effective use of therapeutic and diagnostic ultrasound. Phys. Med. Biol. *34*, 1543–1552.

Foster, K.R., and Wiederhold, M.L. (1978). Auditory responses in cats produced by pulsed ultrasound. J. Acoust. Soc. Am. *63*, 1199–1205.

Franklin, K.B.J., and Paxinos, G. (2007). The Mouse Brain in Stereotaxic Coordinates, Third Edition (New York: Academic Press).

Fry, F.J., Ades, H.W., and Fry, W.J. (1958). Production of reversible changes in the central nervous system by ultrasound. Science *127*, 83–84.

Gavrilov, L.R., Gersuni, G.V., Ilyinsky, O.B., Sirotyuk, M.G., Tsirulnikov, E.M., and Shchekanov, E.E. (1976). The effect of focused ultrasound on the skin and deep nerve structures of man and animal. Prog. Brain Res. *43*, 279–292.

Girardeau, G., Benchenane, K., Wiener, S.I., Buzsáki, G., and Zugaro, M.B. (2009). Selective suppression of hippocampal ripples impairs spatial memory. Nat. Neurosci. *12*, 1222–1223.

Goss, S.A., Johnston, R.L., and Dunn, F. (1978). Comprehensive compilation of empirical ultrasonic properties of mammalian tissues. J. Acoust. Soc. Am. *62*, 423–455.

Goss-Sampson, M.A., and Kriss, A. (1991). Effects of pentobarbital and ketamine-xylazine anaesthesia on somatosensory, brainstem auditory and peripheral sensory-motor responses in the rat. Lab. Anim. *25*, 360–366.

Harvey, E.N. (1929). The effect of high frequency sound waves on heart muscle and other irritable tissues. Am. J. Physiol. *91*, 284–290.

Hayner, M., and Hynynen, K. (2001). Numerical analysis of ultrasonic transmission and absorption of oblique plane waves through the human skull. J. Acoust. Soc. Am. *110*, 3319–3330.

Hira, R., Honkura, N., Noguchi, J., Maruyama, Y., Augustine, G.J., Kasai, H., and Matsuzaki, M. (2009). Transcranial optogenetic stimulation for functional mapping of the motor cortex. J. Neurosci. Methods *179*, 258–263.

Huerta, P.T., and Volpe, B.T. (2009). Transcranial magnetic stimulation, synaptic plasticity and network oscillations. J. Neuroeng. Rehabil. *6*, 7.

Hynynen, K., and Clement, G. (2007). Clinical applications of focused ultrasound-the brain. Int. J. Hyperthermia *23*, 193–202.

Hynynen, K., Clement, G.T., McDannold, N., Vykhodtseva, N., King, R., White, P.J., Vitek, S., and Jolesz, F.A. (2004). 500-element ultrasound phased array system for noninvasive focal surgery of the brain: a preliminary rabbit study with ex vivo human skulls. Magn. Reson. Med. *52*, 100–107.

Hynynen, K., McDannold, N., Clement, G., Jolesz, F.A., Zadicario, E., Killiany, R., Moore, T., and Rosen, D. (2006). Pre-clinical testing of a phased array ultrasound system for MRI-guided noninvasive surgery of the brain—a primate study. Eur. J. Radiol. *59*, 149–156.

Jefferys, J.G., and Haas, H.L. (1982). Synchronized bursting of CA1 hippocampal pyramidal cells in the absence of synaptic transmission. Nature *300*, 448–450.

Kamen, G., and Caldwell, G.E. (1996). Physiology and interpretation of the electromyogram. J. Clin. Neurophysiol. *13*, 366–384.

Kleinfeld, D., Mitra, P.P., Helmchen, F., and Denk, W. (1998). Fluctuations and stimulus-induced changes in blood flow observed in individual capillaries in layers 2 through 4 of rat neocortex. Proc. Natl. Acad. Sci. USA *95*, 15741–15746.

Leighton, T.G. (2007). What is ultrasound? Prog. Biophys. Mol. Biol. *93*, 3–83.

Lele, P.P. (1963). Effects of focused ultrasonic radiation on peripheral nerve, with observations on local heating. Experimental Neurology *8*, 47–83.

Lessmann, V., Gottmann, K., and Malcangio, M. (2003). Neurotrophin secretion: current facts and future prospects. Prog. Neurobiol. *69*, 341–374.

Ludwig, G.D. (1950). The velocity of sound through tissues and the acoustic impedance of tissues. J. Acoust. Soc. Am. *22*, 862–866.

Martin, E., Jeanmonod, D., Morel, A., Zadicario, E., and Werner, B. (2009). High-intensity focused ultrasound for noninvasive functional neurosurgery. Ann. Neurol. *66*, 858–861.

McNamara, J.O. (1994). Cellular and molecular basis of epilepsy. J. Neurosci. *14*, 3413–3425.

Mihran, R.T., Barnes, F.S., and Wachtel, H. (1990). Temporally-specific modification of myelinated axon excitability in vitro following a single ultrasound pulse. Ultrasound Med. Biol. *16*, 297–309.

Morris, C.E., and Juranka, P.F. (2007). Lipid stress at play: Mechanosensitivity of voltage-gated channels. In Current Topics in Membranes, P.H. Owen, ed. (London: Academic Press), pp. 297–338.

Nakashiba, T., Buhl, D.L., McHugh, T.J., and Tonegawa, S. (2009). Hippocampal CA3 output is crucial for ripple-associated reactivation and consolidation of memory. Neuron *62*, 781–787.

NEMA. (2004). Acoustic Output Measurement Standard For Diagnostic Ultrasound Equipment (Washington, DC: National Electrical Manufacturers Association).

Nyborg, W.L. (1981). Heat generation by ultrasound in a relaxing medium. J. Acoust. Soc. Am. *70*, 310–312.

O'Brien, W.D., Jr. (2007). Ultrasound-biophysics mechanisms. Prog. Biophys. Mol. Biol. *93*, 212–255.

Pascual-Leone, A., Valls-Solé, J., Wassermann, E.M., and Hallett, M. (1994). Responses to rapid-rate transcranial magnetic stimulation of the human motor cortex. Brain *117*, 847–858.

Poo, M.M. (2001). Neurotrophins as synaptic modulators. Nat. Rev. Neurosci. *2*, 24–32.

Racine, R.J. (1972). Modification of seizure activity by electrical stimulation. I. After-discharge threshold. Electroencephalogr. Clin. Neurophysiol. *32*, 269–279.

Raymond, S.B., Treat, L.H., Dewey, J.D., McDannold, N.J., Hynynen, K., and Bacskai, B.J. (2008). Ultrasound enhanced delivery of molecular imaging and therapeutic agents in Alzheimer's disease mouse models. PLoS ONE *3*, e2175.

Ressler, K.J., and Mayberg, H.S. (2007). Targeting abnormal neural circuits in mood and anxiety disorders: from the laboratory to the clinic. Nat. Neurosci. *10*, 1116–1124.

Rinaldi, P.C., Jones, J.P., Reines, F., and Price, L.R. (1991). Modification by focused ultrasound pulses of electrically evoked responses from an in vitro hippocampal preparation. Brain Res. *558*, 36–42.

Shealy, C.N., and Henneman, E. (1962). Reversible effects of ultrasound on spinal reflexes. Arch. Neurol. *6*, 374–386.

Szobota, S., Gorostiza, P., Del Bene, F., Wyart, C., Fortin, D.L., Kolstad, K.D., Tulyathan, O., Volgraf, M., Numano, R., Aaron, H.L., et al. (2007). Remote control of neuronal activity with a light-gated glutamate receptor. Neuron *54*, 535–545.

ter Haar, G. (2007). Therapeutic applications of ultrasound. Prog. Biophys. Mol. Biol. *93*, 111–129.

Tsui, P.H., Wang, S.H., and Huang, C.C. (2005). In vitro effects of ultrasound with different energies on the conduction properties of neural tissue. Ultrasonics *43*, 560–565.

Tyler, W.J. (2010). Noninvasive neuromodulation with ultrasound? A continuum mechanics hypothesis. The Neuroscientist, in press. Published online January 25, 2010. 10.1177/1073858409348066.

Tyler, W.J., Alonso, M., Bramham, C.R., and Pozzo-Miller, L.D. (2002). From acquisition to consolidation: on the role of brain-derived neurotrophic factor signaling in hippocampal-dependent learning. Learn. Mem. *9*, 224–237.

Tyler, W.J., Tufail, Y., Finsterwald, M., Tauchmann, M.L., Olson, E.J., and Majestic, C. (2008). Remote excitation of neuronal circuits using low-intensity, low-frequency ultrasound. PLoS ONE *3*, e3511.

Velling, V.A., and Shklyaruk, S.P. (1988). Modulation of the functional state of the brain with the aid of focused ultrasonic action. Neurosci. Behav. Physiol. *18*, 369–375.

Wagner, T., Valero-Cabre, A., and Pascual-Leone, A. (2007). Noninvasive human brain stimulation. Annu. Rev. Biomed. Eng. *9*, 527–565.

White, P.J., Clement, G.T., and Hynynen, K. (2006). Local frequency dependence in transcranial ultrasound transmission. Phys. Med. Biol. *51*, 2293–2305.

Yang, J.F., and Winter, D.A. (1984). Electromyographic amplitude normalization methods: improving their sensitivity as diagnostic tools in gait analysis. Arch. Phys. Med. Rehabil. *65*, 517–521.

Ylinen, A., Bragin, A., Nádasdy, Z., Jandó, G., Szabó, I., Sik, A., and Buzsáki, G. (1995). Sharp wave-associated high-frequency oscillation (200 Hz) in the intact hippocampus: network and intracellular mechanisms. J. Neurosci. *15*, 30–46.

Young, R.R., and Henneman, E. (1961). Functional effects of focused ultrasound on mammalian nerves. Science *134*, 1521–1522.

Zhang, F., Aravanis, A.M., Adamantidis, A., de Lecea, L., and Deisseroth, K. (2007). Circuit-breakers: optical technologies for probing neural signals and systems. Nat. Rev. Neurosci. *8*, 577–581.

Zhang, Y.P., Holbro, N., and Oertner, T.G. (2008). Optical induction of plasticity at single synapses reveals input-specific accumulation of alphaCaMKII. Proc. Natl. Acad. Sci. USA *105*, 12039–12044.

Zhang, S., Yin, L., and Fang, N. (2009). Focusing ultrasound with an acoustic metamaterial network. Phys. Rev. Lett. *102*, 194301–194304.